Queen's University
Belfast

Experimental and Numerical Evaluation of Thermal Performance of Steered Fibre Composite Laminates

Published in:
Heat Transfer – Engineering Applications

Document Version:
Publisher's PDF, also known as Version of record

Queen's University Belfast - Research Portal:
Link to publication record in Queen's University Belfast Research Portal

6

Experimental and Numerical Evaluation of Thermal Performance of Steered Fibre Composite Laminates

Z. Gürdal[1], G. Abdelal[2] and K.C. Wu[3]
[1]Delft University of Technology
[2]Virtual Engineering Centre, University of Liverpool
[3]Structural Mechanics and Concepts, NASA Langley Research Center
[1]The Netherlands
[2]UK
[3]USA

1. Introduction

For Variable Stiffness (VS) composites with steered curvilinear tow paths, the fiber orientation angle varies continuously throughout the laminate, and is not required to be straight, parallel and uniform within each ply as in conventional composite laminates. Hence, the thermal properties (conduction), as well as the structural stiffness and strength, vary as functions of location in the laminate, and the associated composite structure is often called a "variable stiffness" composite structure. The steered fibers lead not only to the alteration of mechanical load paths, but also to the alteration of thermal paths that may result in favorable temperature distributions within the laminate and improve the laminate performance. Evaluation of VS laminate performance under thermal loading is the focus of this chapter. Thermal performance evaluations require experimental and numerical analysis of VS laminates under different processing and loading conditions. One of the advantages of using composite materials in many applications is the tailoring capability of the laminate, not only during the design phase but also for manufacturing. Heat transfer through variable conduction and chemical reaction (degree of cure) occurring during manufacturing (curing) plays an important role in the final thermal and mechanical performance, and shape of composite structures.

Three case studies are presented in this chapter to evaluate the thermal performance of VS laminates prior to and after manufacturing. The first case study is a numerical analysis that investigates the effect of variable conductivity within the VS laminate on the temperature and degree of cure distribution during its cure cycle. The second case study is a numerical analysis that investigates the transient thermal performance of a rectangular VS composite laminate. Variable thermal conductivity will affect the temperature profile and results are compared to a unidirectional composite. The effect of fiber steering on transient time and steady state solutions is compared to the effect of unidirectional fibers. The third case study is an experimental one that was conducted to evaluate the thermal performance of two variable stiffness panels fabricated using an Advanced Fiber Placement (AFP) Machine.

These variable stiffness panels have the same layup, but one panel has overlapping bands of unidirectional tows (which lead to thickness variations) and the other panel does not. Results of thermal tests of the variable stiffness panels are presented and compared to results for a baseline cross-ply panel. These case studies will show the impact of the steering parameters of variable stiffness laminates during the manufacturing and design phases.

2. Preliminaries

Laminated composite plates structures, which have high strength-to-weight and stiffness-to-weight ratios, are extensively used in aerospace and automotive applications that are exposed to elevated temperatures. Accurate knowledge of the thermal response of these materials is essential for the optimum design of thermal protection systems. In some circumstances, high thermally induced compressive stresses may be developed in the constrained plates and can therefore lead to buckling failures. In addition, conductivity of the fiber-reinforced layers is direction dependent, and therefore the degree of anisotropy of the laminate can substantially influence the conductivity of the laminate in different directions.

Variable stiffness laminates with steered fiber paths offer stiffness tailoring possibilities that can lead to alteration of load paths, resulting in favorable temperature distributions within the laminate and improved laminate structural performance. A further generalization of this idea was to allow the direction of the fiber orientation angle variation to be rotated with respect to the coordinate direction x, rather than limiting it to be only along the x-axis or the y-axis. As shown in Figure 1, a fiber orientation angle T_0 is defined at an arbitrary reference point A with respect to direction x' that is rotated by an angle ϕ from the coordinate axis x. The fiber orientation angle is then assumed to reach a value T_1 at point B located a characteristic distance d from point A. With the linear variation of the fiber orientation angle between the points A and B, the equation for the fiber orientation angle along this reference path takes the form,

$$\theta(x') = \phi + (T_1 - T_0)\frac{|x'|}{d} + T_0 \tag{1}$$

A variable stiffness layer can be represented with three angles and a characteristic distance to represent a single layer. Assuming the characteristic distance to be associated with a geometric property of the part, representation of a single curvilinear layer may be specified by $\phi<T_0|T_1>$. A conventional representation, a $\pm$ sign in front of either ϕ or $<T_0|T_1>$ means that there are two adjacent layers with equal and opposite variation of the fiber orientation angle. A laminate with $\pm \phi \pm<T_0|T_1>$ designation will have four curvilinear layers: a $\pm \phi$ $<T_0|T_1>$ pair along the $+\phi$ direction, and a $\pm \phi <T_0|T_1>$ pair along the $-\phi$ direction.

Variable stiffness (VS) laminates were introduced by (Gürdal and Olmedo, 1993; Olmedo and Gürdal, 1993). Examples of fiber orientation angle tailoring include theoretical and numerical studies by (Banichuk, 1981; Banichuk and Sarin, 1995), (Pedersen, 1991, 1993)], and (Duvaut et al., 2000). In a design study by (Gürdal et al., 2008), analyses of variable stiffness panels for in-plane and buckling responses are developed and demonstrated for two distinct cases of stiffness variation. Later optimization studies (Setoodeh et al., 2006, 2007, 2009) were carried out demonstrating the theoretical benefits of variables stiffness laminates in improving structural performance. For variable stiffness laminates, which also

have spatially variable coefficients of thermal expansion along with the stiffness properties, spatial variation of residual stresses are induced. More recent studies investigated the effect of thermal residual stresses on the mechanical buckling performance of variable stiffness laminates (Abdalla et al., 2009).
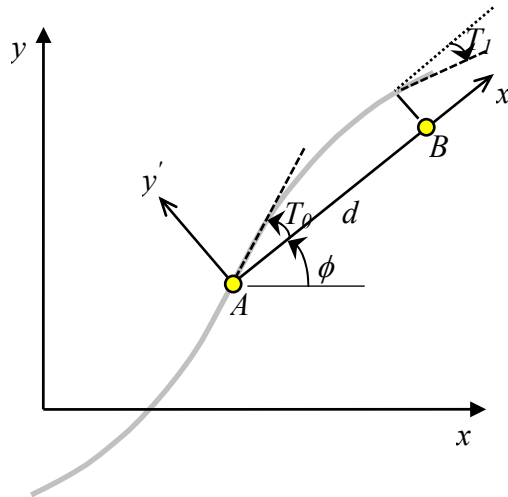

Fig. 1. Reference path definition of a variable layer

The degree of damage and strength degradation of the VS laminates subjected to severe thermal environments is a major limiting factor in relation to service requirements and lifetime performance. In order to predict these thermally induced stresses, a detailed understanding of the transient temperature distributions is essential. A number of studies of isotropic materials and composites have been carried out to explore the potentially complicated time dependence of the temperature field (Hetnarski, 1996). There have also been numerous analytical models developed over the years to describe the transient behaviors of commonly encountered geometries (Mittler et al., 2003; Obata and Noda, 1993).

Alternatively, in order to endure the severe thermal loads, many structural components are made such that they are non-homogeneous. Thermal barrier coatings of super alloys on ceramics used in jet engines, stainless steel cladding of nuclear pressure vessels, and a great variety of diffusion-bonded materials used in microelectronics may be mentioned as some examples. Typically, these non-homogeneous materials and structures are subjected to severe residual stresses upon cooling from their processing temperatures. They may also undergo thermal cycling during operations. Depending on the temperature gradients, the underlying thermal stress problem may be treated as a thermal shock problem or as a quasi-static isothermal problem in the sense that the problem may still be time-dependent but with no variation of temperature within the composite solid.

Clearly, there is an actual need for investigating the thermal transients developed within VS composites. However, because of the inherent mathematical difficulties, thermal analyses of non-homogeneous structural materials are considerably more complex than in the corresponding homogeneous case. Numerical techniques such as the finite element method

are of great importance for solving for temperature profile and stress distribution in VS laminates.

3. Numerical heat conduction analysis

The main purpose of this section is to study a finite-element approximation to the solution of the transient and steady-state heat conduction with different boundary conditions in a two-dimensional rectangular region. A Galerkin finite element formulation is applied to the 2-D heat conduction equation using four planar finite elements. The composite conduction and capacitance matrices are derived as functions of the steered fiber orientation angles.

3.1 Two-dimensional heat conduction in Cartesian coordinates

The governing differential equation for a two dimensional heat conduction problem is given by,

$$k_x \, T_{,xx} + k_y \, T_{,yy} + Q = \rho \, c_p \, T_{,t} \tag{2}$$

where T is the temperature, k_x and k_y are material conductivity along the x- and y-directions, ρ is material density, Q is the inner heat-generation rate per unit volume, and c_p is material heat capacity.

Boundary conditions are described as,

$$
\begin{aligned}
&T = T_0\big|_{S=S1} \quad \text{(specified temperature)} \\
&k_x \, T_{,x} + k_y \, T_{,y} = q\big|_{S=S2} \quad \text{(specified heat flow)} \\
&k_x \, T_{,x} + k_y \, T_{,y} = h(T_s - T_e)\big|_{S=S3} \quad \text{(convection boundary condition)}
\end{aligned}
\tag{3}
$$

where h is the convection coefficient, Ts is an unknown surface temperature, Te is a convective exchange temperature, and q is the incident heat flow per unit surface area.

3.2 Heat conduction simulation using finite element

Using a typical Galerkin finite element approach to Eqn. (2) the residual equation for a plate with unit thickness assumes the form,

$$\iint [N] \big[k_x \, T_{,xx} + k_y \, T_{,yy} + Q - \rho \, c_p \, T_{,t} \big] \, dx \, dy = 0 \tag{4}$$

where the temperature field function is expressed in terms of the interpolation functions as,

$$[T] = [N][T]^e \tag{5}$$

Integration of Eqn. (4) by parts yields,

$$
\begin{aligned}
&\iint \Big[[N_{,x}]^T k_x [N_{,x}] + [N_{,y}]^T k_y [N_{,y}] \Big] \, dx \, dy \, \{T\}^e + \\
&\rho \, c_p \iint [N]^T [N] \, dx \, dy \, \{T_{,t}\} + \int_V Q \, N_i \, dV = \int [N]^T q \, dS
\end{aligned}
\tag{6}
$$

where q is the heat flow through unit area. Finally the governing equation takes the form,

$$\left[K_T + K_h\right]\ \{T\}\ +[C]\ \{\dot{T}\}\ =\ \{F_T\}\ +\{R_Q\}+\{R_h\} \tag{7}$$

where,

$$[K_C]\ =\ \text{composite conduction matrix,}\ Watt\ /\ C^{\circ}\ =\ \int_V N^T\ [k]\ N\ dV$$

$$[K_h]\ =\ \text{composite convection matrix,}\ Watt\ /\ C^{\circ}\ =\ \int_{S3} h\ N^T\ N\ dS$$

$$\{T\}\ =\ \text{unknown nodal temperature vector,}\ C^{\circ}.$$

$$[C_T]\ =\ \text{capacitance matrix, J/}C^{\circ}\ =\ \int_V \rho\ c_p\ N^T\ N\ dV$$

$$\{\dot{T}\}\ =\ \partial\{T\}^e/\partial\, t$$

$$\{F_T\}\ =\ \text{composite element nodal force vector, Watt}\ =\ \int_V N^T\ q_s\ dS$$

$$\{R_Q\}\ =\ \text{internal-heat vector,}\ Watt\ /\ m^3\ C^{\circ}\ =\ \int_V Q\ N^T\ dV$$

$$\{R_h\}\ =\ \text{convection heat vector,}\ Watt\ /\ m^2\ C^{\circ}\ =\ \int_{S3} h\ T_e\ N^T\ dS$$

$$N\ =\ \text{interpolation function,}\ \{T\} = [N]\{T\}^e$$

Introducing the normalized lamination parameters [Gürdal et al., 1999],

$$\{V_1, V_2, V_3, V_4\} = \int_{-1/2}^{1/2} \{\cos 2\theta, \sin 2\theta, \cos 4\theta, \sin 4\theta\} d\overline{z}$$

$$\{W_1, W_2, W_3, W_4\} = 12\int_{-1/2}^{1/2} \overline{z}^2 \{\cos 2\theta, \sin 2\theta, \cos 4\theta, \sin 4\theta\} d\overline{z} \tag{8}$$

the conductivity matrix [k] can be expressed as a function of the lamination parameters,

$$[k]\ = K_0 + K_1\ V_1 + K_2\ V_2 \tag{9}$$

$$K_0 = \begin{bmatrix} 0.5(k_{11}+k_{22}) & 0 \\ 0 & 0.5(k_{11}+k_{22}) \end{bmatrix} \qquad K_1 = \begin{bmatrix} 0.5(k_{11}-k_{22}) & 0 \\ 0 & 0.5(k_{11}-k_{22}) \end{bmatrix}$$

$$K_2 = \begin{bmatrix} 0 & 0.5(k_{22}-k_{11}) \\ 0.5(k_{22}-k_{11}) & 0 \end{bmatrix} \tag{10}$$

where k_{11} and k_{22} are the conductivity of the lamina along and perpendicular to the fibers directions respectively.

The finite element solution of time-dependent field problems produces a system of linear first-order differential equations in the time domain. These equations must be solved before the variation of the temperature T in space and time is known. There are several procedures for numerically solving Eqn. (7). Finite difference approximation (central difference) in the time domain is applied to generate a numerical solution,

$$\left([C_T]+\frac{\Delta t}{2}[K_T]\right)\{T\}_{i+1} = \left([C_T]-\frac{\Delta t}{2}[K_T]\right)\{T\}_i + \frac{\Delta t}{2}\left(\{F_T\}_i + \{F_T\}_{i+1}\right) \tag{11}$$

If Δt (time increment) and the material properties are independent of time, Eqn. (11) can be formulated as,

$$[A]\{T\}_{i+1} = [P]\{T\}_i + \{F^*\}$$

(12)

where [A] and [P] are combinations of [C] and [K], and $\{F^*\} = \dfrac{\Delta t}{2}\left(\{F_T\}_i + \{F_T\}_{i+1}\right)$.

3.3 Numerical stability techniques

Transient heat conduction problems can be solved by first discretizing the spatial dimensions using the finite element method, then transforming the space-time partial differential equation (PDE) into an ordinary differential equation (ODE) in time. The time integration of the discrete Eqn. (7) is then performed using ODE integrators. These integrators replace the time derivative by a finite difference approximation (forward, central, or backward differences). This integration method is inexpensive per step, but numerical stability requires using small time-steps. The numerical oscillations in the values of {T} from one time-step to the next are related to $[A]^{-1}[P]$, and can be avoided by applying the following criteria (Segerlind, 1984),

$$\det\left([C_T]^e - \delta[K_T]^e\right) = 0$$
$$\Delta t \ < \ 2\,\delta$$

(13)

(Trujillo, 1977) has proposed an explicit algorithm that has a time-step fifteen times greater than the conventional method used. (Hughes et al., 1982) proposed an element-by-element implicit algorithm to solve Eqn. (7). (Zienkiwicz et al., 1980) proposed a procedure based on systemic partitioning of the discrete Eqn. (7) and involving extrapolation.

4. Curing simulation of variable stiffness laminate

Thermoset polymers often release a significant heat of reaction during processing. The chemical reaction that occurs during the curing of thermoset polymers plays an important role in the process modeling of thermoset composites. The exothermic heat released during the curing process can cause excessive temperatures in the interior of composites. Cure kinetics that provide information on the curing rate and the amount of exothermic heat release during the chemical reaction are important in the process simulation of composite materials with thermoset polymers. Therefore, the inclusion of an accurate cure kinetics model is essential for the processing simulation of thermoset composites. Several studies have shown that amine-cured epoxy resins are governed by an autocatalytic reaction (Johnston, 1997; Scott, 1991). The epoxy group that reacts with a primary amine produces a secondary amine and then forms a tertiary amine. These reactions are also accelerated by the catalytic action of the hydroxyl group that is formed as a by-product of the amine–epoxy reaction.

The majority of heat transfer models for composites processing consider heat flow in the through-thickness direction only (a one-dimensional model) or make the even simpler assumption of a uniform laminate temperature (White and Hahn, 1992). More sophisticated

models examining heat transfer in two and three dimensions have also been developed (Bogetti and Gillespie, 1991). The resin chemical reaction is generally indicated by a time-dependent measure known as the degree of cure, α, as in Equation (14) which is usually defined based on a measure of the heat given off by bond formation as follows:

$$\alpha = \frac{1}{H_R} \int_0^t \left(\frac{dq}{dt} \right) dt \tag{14}$$

where (*dq/dt*) is the rate of heat generation and H_R is the total amount of heat generated per unit volume during a full reaction. The value of α can be easily determined using standard differential scanning calorimetry (DSC) heat flow measurements. The heat generated due to cure of the resin Q* is expressed as,

$$Q^{\bullet} = \rho \, H_R \, \frac{d\alpha}{dt} \tag{15}$$

where *da/dt* is designated as the cure rate and ρ is the composite material density.

A number of different models have been proposed to simulate the cure kinetics of various resin systems. These models can be divided into two general types: mechanistic and empirical. Mechanistic models use as their basis a detailed understanding of the chemical reactions that take place throughout the cure process. Such models are not always practical due to the complexity of the chemical reactions that can vary greatly from one resin system to another depending on the combination of base resin, hardeners and catalysts. Furthermore, most commercial resin systems are proprietary and the user is often prohibited from even trying to determine their exact composition. Empirical models are expressions derived to provide a fit to experimentally determined cure rates. Most cure models employ Arrhenius-type equations, with the rate of reaction expressed as some function of degree of cure and temperature. An example of a commonly used semi-empirical expression for cured epoxy systems is (Scott, 1991):

$$\frac{d\alpha}{dt} = \left(Y_1 + Y_2 \, \alpha^m \right) \left(1 - \alpha \right)^n$$
$$Y_i = A_i \, \exp\left(-\Delta E_i / RT \right) \tag{16}$$

where ΔE_i are activation energies, R is the gas constant, and A_i, m, n are experimentally-determined constants. To account for the effect of glass transition on reaction rate, a combination of expressions of the form of Eqns. (16) (Lee et al., 1982; White and Hahn, 1992) and modified expressions of similar type have been used (Dusi et al., 1987; Cole et al., 1991).

$$\frac{d\beta}{dt} = \left(Y_1 + Y_2 \, \beta^m \right) \left(1 - \beta \right)^n \tag{17}$$

where Y_i are defined as in Eqn. (16) and *m* and *n* are other experimentally determined constants. The parameter β is the "isothermal degree of cure", defined as the limiting degree of cure at a given temperature. Its relation to the degree of cure is given by:

$$\alpha = \beta \, \frac{H_T(T)}{H_R} \tag{18}$$

where $H_T(T)$ is the total amount of heat that would be given off by isothermally curing the resin at temperature T for infinite time.

4.1 Thermal-chemical model

A thermo-chemical model simulation requires the determination of the reaction kinetics of each resin and thermal transport of the heat of reaction across the laminate panel to calculate changes in the laminate temperature that affect thermal strains, and degree of cure that affects resin modulus. The following mathematical equation is modeled applying transient thermal analysis.

$$\rho c_p \frac{\partial T}{\partial t} = \frac{\partial}{\partial x_i}\left(k_{ij}\frac{\partial T}{\partial x_j}\right) + \rho H_R \frac{\partial c}{\partial t} + Q_v$$

$$(i,j = 1,2)$$

(19)

where ρ denotes the composite density, c_p the specific heat, T the temperature, t the time, x_i the spatial coordinates, and k_{ij} the components of the thermal conductivity tensor. The degree of cure c is defined as the ratio of the heat released by the reaction to the ultimate heat of reaction H_R, and Q_v is the heat convection to the surrounding air in the autoclave. Orthotropic conductivity is assumed for all materials so that values of k_{11}, k_{22}, and k_{33} are required. Assuming resin conductivity is isotropic and fibre conductivity is transversely isotropic, a rule of mixture is used (Twardowski et al., 1993) to evaluate lamina thermal conductivity:

$$K_{11} = V_f.K_{f11} + \left(1 - V_f\right)K_r$$

$$K_{22} = K_r.\left[\left(1 - 2.\sqrt{\frac{V_f}{\pi}}\right) + \left(\frac{1}{B}\right).\left[\pi - \left(\frac{4}{\sqrt{1 - B^2.\frac{V_f}{\pi}}}\right).a\tan\left(\frac{\sqrt{1 - B^2.\frac{V_f}{\pi}}}{1 + B.\sqrt{\frac{V_f}{\pi}}}\right)\right]\right]$$

$$B = 2.\left[\left(\frac{K_r}{Kf_{22}}\right) - 1\right]$$

(20)

where K_{f11}, K_{f22} are the longitudinal and transverse conductivities of the fibers, and K_r is the isotropic conductivity of the resin. These values are assumed as a function of temperature. Laminate global conductivity is calculated as described in eqn. (9) and eqn. (10).

The lamina specific heat capacity is calculated using the following equation (Gürdal et al., 1999),

$$C_p = \frac{V_f C_{pf}\rho_f + \left(1 - V_f\right)C_{pr}\rho_r}{V_f\rho_f + \left(1 - V_f\right)C_{pr}\rho_r}$$

(21)

where C_{pf} and C_{pr} are the respective specific heats of the fibers and resin, and are modelled as a function of temperature. The internal heat generated due to the exothermic cure reaction is described as in (White and Hahn, 1992),

$$\frac{dc}{dt} = Y\alpha^m (1-\alpha)^n$$

$$Y = Ae^{-\Delta E/RT}$$

(22)

where Y is the Arrhenius rate, R=8.31 J/Mol.K is the universal gas constant, A the frequency factor, (*m*, and *n)* are experimentally-determined constants for a given material, and ΔE the activation energy. The heat transfer coefficient for an autoclave of size (1.8 m x 1.5 m) is measured and can be expressed as (Johnston, 1997),

$$h = 20.1 + 9.3 \ (10^{-5}) \ P \quad (W/m^2 \ K)$$

(23)

where P is the autoclave pressure.

4.2 Cure simulation using finite elements

A thermochemical model is used for calculation of temperature and the degree of cure in composite components. Accurate prediction of these parameters is potentially useful to the composites modeling in a number of ways. First of all, one of the main objectives of processing thermoset composite materials is to achieve uniform cure of the matrix resin so that a structure can attain its maximum stiffness, static and fatigue strength and resistance to moisture and chemical degradation. Achieving maximum degree of cure in minimum time would seem to indicate that a high temperature cure cycle be used. However, this approach has other, potentially negative, implications for the cure process. For example, the rapid heat evolution of the resin's exothermic reaction at high temperatures can lead to a 'runaway' reaction as heat is generated more quickly than it can be removed, potentially resulting in resin thermal degradation. It has also been found that the large spatial and temporal gradients in resin degree of cure and temperature induced by rapid cure can be an important source of process-induced stress (Levitsky and Shaffer, 1975; Bogetti, 1989), especially in thick-section composites. Thermochemical model predictions are also important to the simulation of other processing phenomena such as resin flow and the generation of residual stress and deformation. One reason this is so is that temperature and degree of cure are two of the most important 'state' variables used to predict composite material properties during processing. Thus, prediction of everything from resin viscosity to thermal expansion and resin cure shrinkage strains are dependent on thermochemical model predictions.

The thermochemical model consists of a combination of analyses for heat transfer and resin reaction kinetics. The model of (Bogetti and Gillespie, 1992) can be applied to general two-dimensional composite modeling. It has the added capability of incorporating multiple composite and non-composite materials as well as process tooling. Other important features include the potential for improved boundary condition modeling using the autoclave simulation and consideration of material property variation during processing. Also, by integrating another model that considers resin flow, the effect of fiber volume fraction variation during processing can also be considered.

The governing equation of the thermochemical model is the unsteady-state two-dimensional anisotropic heat conduction equation with an internal heat generation term from the resin's exothermic curing reaction is modeled using Eqn. (19). The governing equations of the heat transfer portion of the problem are solved employing the finite element approximation, and

time integration is performed as described in section 3.3 using a central finite difference approximation.

The heat transfer equation, Eqn. (19), and the cure kinetics equations outlined in section 4.1 are coupled. Ideally, therefore, a coupled solution technique would be employed in which both temperature and degree of cure would be solved in a single calculation. For the current model, for each time increment, the temperature will be solved first at the discretized locations (nodes) using the previous increment degree of cure (internal heat) and applied boundary conditions. Then using the calculated temperature, the degree of cure and the new internal heat generated are updated using Eqn. (22). Composite thermal properties that are used in our simulation are listed in Table 1.

Specific heat capacity (J/Kg.K)	C_{pf} = 800
Thermal conductivity (W/m.K)	k_{fl} = 6.5 k_r = 0.65
Fibre volume fraction	V_f = 0.6
Cure kinetic model	H_R = 590(10³), ΔE = 66.9 KJ/gmole, A =5.333E+5 /s, m=0.79, n=2.16, α_0=0.01

Table 1. Thermal material properties.

Boundary conditions considered on the two-dimensional simulation analysis are:

- *Convective heat transfer (applied on the top surface of the laminate)* ($q = h$ (T_e-T), where *h* is the heat transfer coefficient (see Eqn. (23)) and *Te* and *T* are the air and boundary temperatures, respectively). Convective heat transfer is usually the dominant heat transfer mechanism in an autoclave at temperatures normally encountered in thermoset processing.
- Adiabatic boundary (along the laminate's edges) (q = 0 or $\partial T/\partial n$ = 0, where n is the surface normal vector).

4.3 Numerical results

The composite plate considered in this study is a mid-plane symmetric laminate with dimensions (0.36m x 0.36m x 0.003m). It consists of 6 sub-laminates, each of which consists of 4 layers [$\pm\phi\pm<T_0|T_1>$], for a total of 24 plies. The laminate is made from carbon/epoxy (AS4/3501) with material properties defined in Table 1. The analysis is performed by discretizing the panel using a uniform mesh of rectangular four-noded Kirchhoff plate elements. The transient response of the VS laminate and the different shape of the heat transfer channels from the straight-fiber ones (to be discussed in the next section), could affect both the temperature and degree of cure response. However, performance of the simulation as a function of the autoclave time cycle showed that there is no difference in thermal performance "in autoclave" between VS and straight fiber composites.
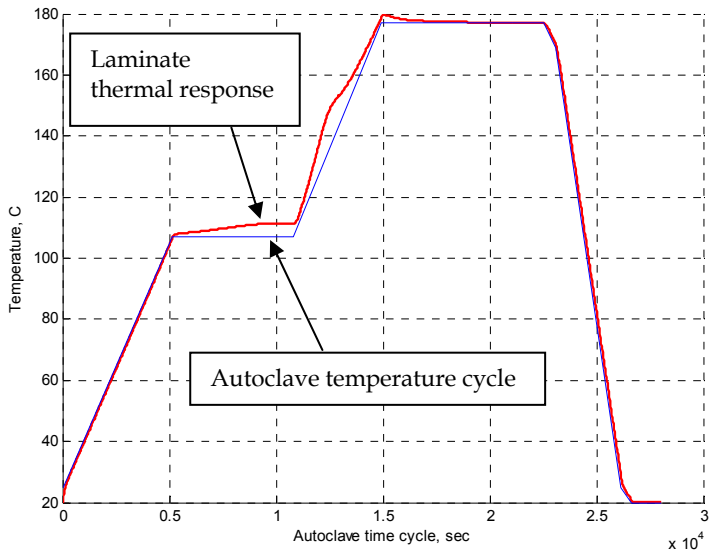
Fig. 2. Autoclave temperature cycle and temperature response of composite.
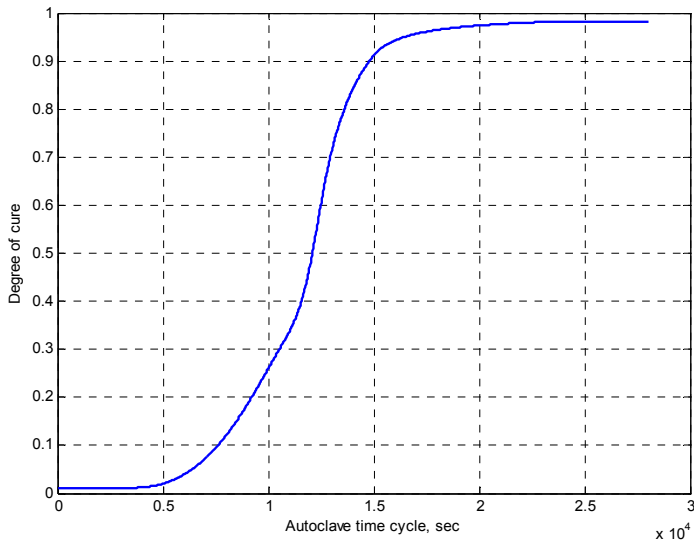

Fig. 3. Degree of cure of VS and straight-fiber composite.

The autoclave temperature cycle and the laminate thermal response at the composite plate center are shown in Figure 2. The autoclave thermal cycle can be divided to three phases. The first phase involves raising the autoclave air temperature from room temperature (25 °C) to 107 °C, and then holding this temperature for 1 hour. The second phase raises the autoclave air temperature to 177 °C and holds this temperature for 2 hours. The heat that is

generated by the cure kinetics during the autoclave thermal cycle starts when the composite panel temperature is close to 107 °C. This internal heat leads to an increase in the composite panel temperature, then the extra heat is transferred back to the autoclave air. Once the epoxy is fully cured, there is no exothermic curing heat reaction. The degree of cure is shown in Figure 3 as a function of the cure cycle time. The change in the degree of cure is low during the initial phase of the autoclave thermal cycle, once the exothermic curing reaction started, we can see faster curing until the autoclave air temperature is 177 °C, then curing slows down until it is fully cured. The main factor behind the similarity of curing of VS and straight fibers is the composite panel is exchanging heat through the transverse direction and not through the in-plane direction (as boundaries are isolated). Heat exchange through boundaries will be affected by the in-plane fiber layout and is discussed in next section.

5. Transient heat response of variable stiffness laminate

Clearly, there is an actual need for investigating the thermal transients developed within VS composites. However, because of the inherent mathematical difficulties, thermal analysis of non-homogeneous structural materials is considerably more complex than in the corresponding homogeneous case. Numerical techniques such as finite element methods are of great importance for solving for temperature profile and stress distribution.

This section investigates thermal transient analysis of rectangular variable stiffness composite under uniform partial heat flux using finite element analysis. Variable thermal conductivity will affect the temperature profile results compared to unidirectional composite. The effect of the extra design parameter of variable stiffness laminates (steering of fibers) on transient response is investigated. The need for cooling of a structural panel is determined by transient time and boundary conditions. The transient solution of variable stiffness laminate is compared to the unidirectional one. Later, the steady state temperature profile is used to determine thermal stresses of the variable stiffness laminate compared to a unidirectional one applying forced straight edge boundary conditions. The mechanics of variable-stiffness laminates are discussed in (Abdalla et al., 2009).

5.1 Transient response

A two-dimensional finite element (FE) model describing heat transfer analysis of a variable-stiffness composite laminate exposed to partial surface heating is illustrated in Figure 4. The effect of fiber steering (T_0, T_1) on transient time and steady state solution is compared to straight fibers. A Matlab computer program was written for the FE procedure discussed in previous sections. The program has been used to evaluate the transient response of different fiber steering. Material properties of the laminate are listed in Table 1. The composite wall is assumed to have a uniform initial temperature; $T_i = 0$ °C. The results presented here are for a partially heated plate at input heat energy of $h_{Input} = 100$ W/(m²). The accuracy of the results was verified by comparing the straight-fiber results to the ABAQUS transient heat transfer analysis. Boundary conditions for laminate edges act as a heat sink and are fixed at $T = 0$ °C. The transient response of a heat conduction problem can be characterized by two parameters. One parameter is the time to reach steady state. A longer time to reach steady state is better for thermal protection panels as it allows more time for the structure to absorb heat, which reduces thermal stresses and delays the ablation process that degrades material properties. The second parameter is the maximum temperature reached at the center of the

panel. A lower maximum temperature is desirable for the same reasons to reduce thermal stresses, which improves buckling response and delays the ablation process. A variable stiffness laminate adds more three design parameters (ϕ, T_0, T_1) that can be used to achieve the optimal thermal performance. For example, Figure 5 compares the performance of variable stiffness panels while varying T_0 and T_1 versus the straight-fiber laminate performance. The transient time is normalized by the maximum transient time that can be achieved using a straight-fiber laminate, and the maximum temperature at plate center is normalized by the minimum temperature achieved using a straight-fiber laminate. The straight-fiber laminate is represented by the heavy line, and is a symmetric angle-ply layup that has a linear variation of a pair of fiber angles $[\pm\theta]_s$, so the 0° and 90° laminates have the same maximum temperature and transient time. The performance changes only in the range between 0° and ±45° degrees, and appears to be nearly linear with constant transient time, and independent of the orientation angle. The maximum temperature for the 0° and 90° laminates is about 1.3 times that of the minimum temperature, which is achieved for the ±45° laminate.
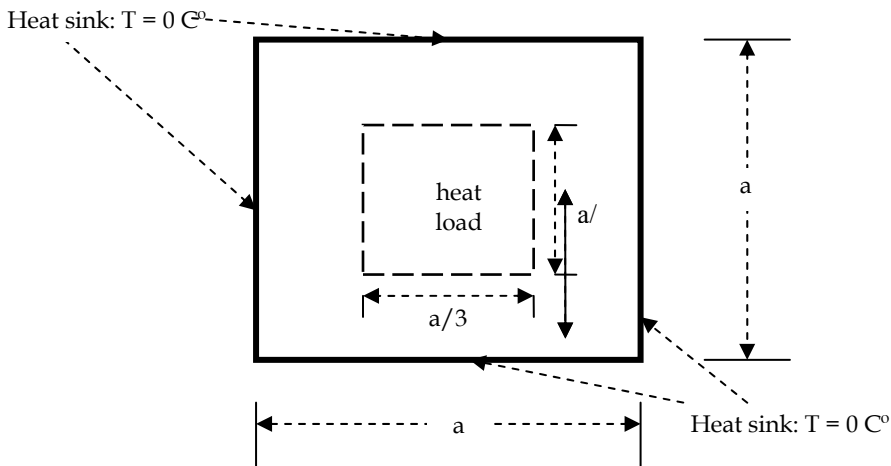
Fig. 4. Square variable stiffness panel under thermal load.

Two types of variable stiffness laminates are studied. A type-1 laminate, which is represented by $[0\pm<T_0/T_1>]_{2S}$, is constructed of layers with steered fiber orientation angles θ which are a function of x-coordinate only. Type-2, which is represented by $[0\pm<T_0/T_1>/90\pm<T_0/T_1>]_S$, is constructed with half of the layers having fiber orientations which are functions of the x-coordinate, and the other half functions of the y-coordinate. The type-1 laminate performance is presented by incrementally changing T_1 in the range of 0° to 90°. For each increment of T_1, T_0 is varied between 0° and 90°, and then the normalized maximum temperature is plotted versus the normalized transient time in Figure 5. The minimum temperature at the plate center is achieved at $[T_1=0, T_0=60]$. The longest transient time is achieved for the VS lamina with $[T_1=90, T_0=0]$. Incrementing T_1 of the VS laminate leads to higher temperatures at the plate center and higher transient times. This result can be explained by the fact that the heat is easily channeled when the fiber angle at the plate edges (T_1) is perpendicular to the plate boundaries. The lowest heat flux is achieved at $T_1=0°$,

where fibers at plate edges are tangent to boundaries. Changing the stacking sequence of the variable stiffness laminate to type-2, where $[0 \pm <T_0/T_1>/90\pm <T_0/T_1>]_S$ leads to a minimum temperature at the plate center at $[T_0=75^o, T_1=0^o]$.
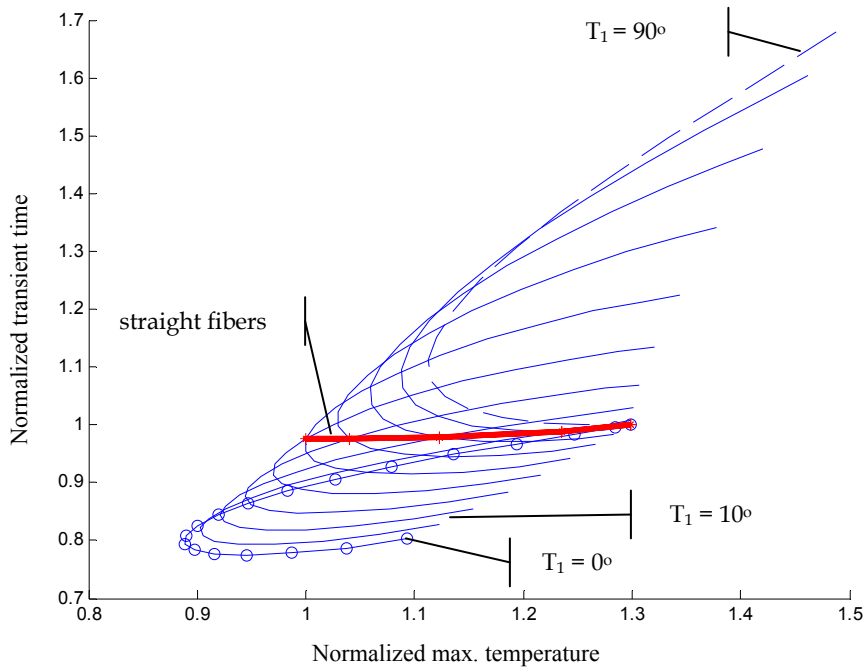

Fig. 5. Transient time and maximum temperature for straight-fibers, type-1 $[0\pm<T_0|T_1>]_{2s}$

The steady-state heat flux is studied to investigate the effect of varying fiber paths for selected design configurations from Figure 5. Steady state temperature and transient time are controlled by heat dissipation along two channels, along the longitudinal and transverse directions of the composite plate. The heat dissipation profile is dependent on the fiber orientation angle in the laminate, as the fibers are more conductive than the matrix. A comparison of the heat flux profile for two straight-fiber laminates $[0]_{2S}$ and $[\pm45]_{2S}$ is shown in Figures 6 and 7. For the laminate with fiber angle $\theta=0^o$, the heat is dissipated only along x-direction, while the $[\pm45]_{2S}$ laminate dissipates heat in two directions, which promotes lower temperatures and smaller transient times. As shown on Figure 6, the normalized heat channel along the x-direction where $\theta=0^o$ is broader from the one where $\theta=\pm45^o$, which has an extra heat channel along the y-direction. The heat flux for the $[0\pm<60/0>]_{2S}$ laminate is shown in Figure 8. Clearly, the laminate has more heat channels along the longitudinal and transverse direction than the $\theta=\pm45^o$ laminate, which leads to 20% less transient time and 12% less maximum temperature at plate center, as shown on Figure 5.

Next, plots of heat flux for one quarter of the plate for the $\theta=0^o$ straight-fiber laminate, $[0\pm<45/0>]_{2S}$, and $[0\pm<60/0>]_{2S}$ laminates are shown in Figure 9 and Figure 10. These figures indicate that the straight fibers at $\theta=0^o$ have the highest heat flux along the x-direction, and the lowest along the y-direction. The heat flux for the $[0\pm<60/0>]_{2S}$ laminate has two heat

channels along the x- and y-directions, and both dissipate heat higher than the $\theta=\pm45^{\circ}$ laminate. The success of the variable stiffness laminate in dissipating heat faster and reaching a lower temperature compared to the straight-fiber laminate prompted the idea of introducing the second laminate type in which the fiber orientation is steered in both the x- and y-directions. The heat flux plots indicate that the variable stiffness laminate has the best characteristics in the x- and y-directions.
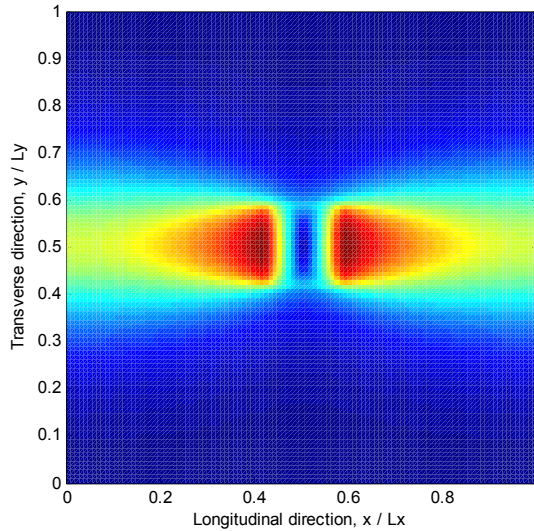
Fig. 6. Heat Flux for 0° straight angle laminate.
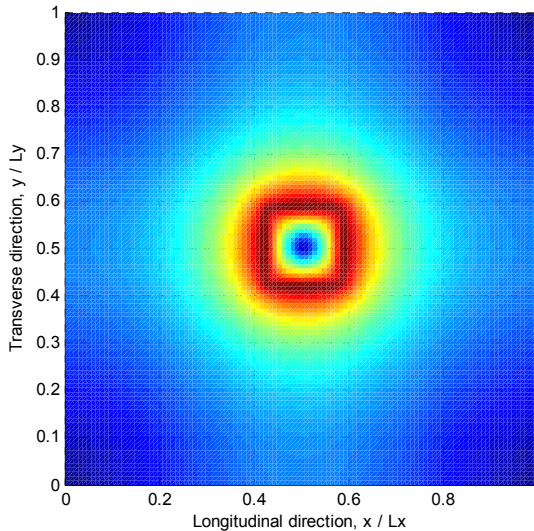
Fig. 7. Heat Flux for $\pm45^{\circ}$ straight angle laminate.
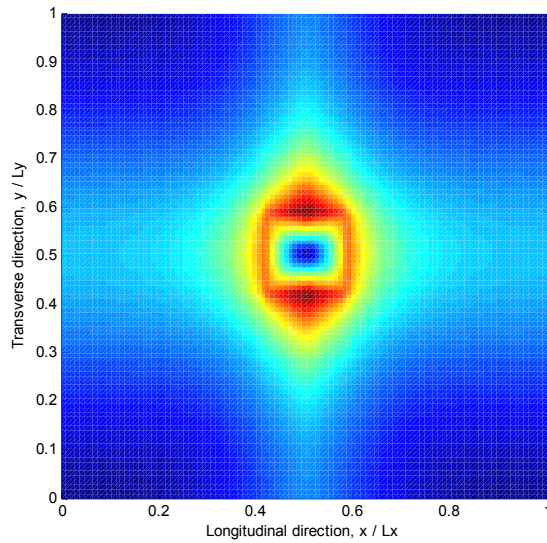
Fig. 8. Heat Flux for [*0 ±<60/0>*]$_{2S}$ VS laminate.
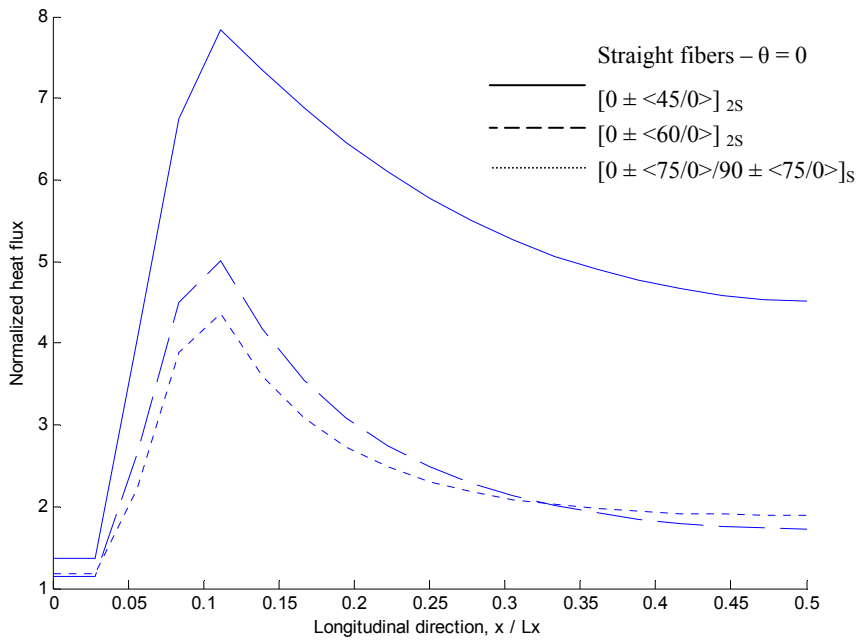
Fig. 9. Heat Flux along longitudinal direction for one-quarter of plate

Steering the fibers provides an additional design parameter to control both the transient time and temperature profile. Incrementing T_1 of the steered fibers leads to a higher

transient time and temperature at plate center, while incrementing T_0 has opposite effect in the range of $T_0=0^\circ$ to 60°. Next, the stress resultants and plane deformations are examined for two types of stacking sequences under forced straight edge boundary conditions (where nodes that are located on the laminate edge are coupled with one selected node to force equal displacements).
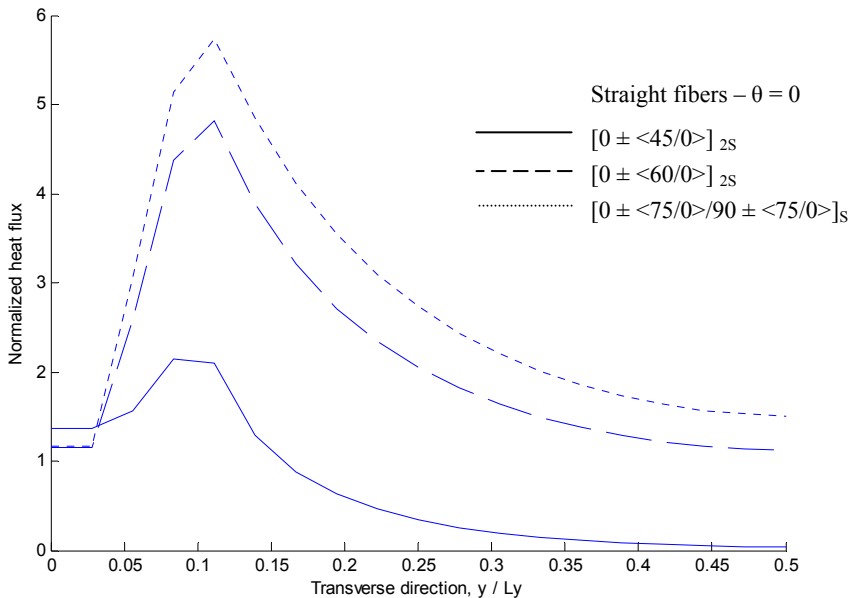
Fig. 10. Heat Flux along transverse direction for one-quarter of plate

5.2 Steady state stress results

The in-plane response of the two types of laminates, $[0\pm<T_0|T_1>]_{2S}$ and $[0\pm<T_0/T_1>/90\pm<T_0/T_1>]_S$ (type 1 and type 2, respectively), are considered under a steady-state temperature input. Under an applied non-uniform temperature profile, one or both of the in-plane stress and displacement distributions can be highly non-uniform, which results from the coupling of the in-plane equilibrium equations. An in-plane analysis of a variable stiffness laminate is important because one has to determine the location of the largest stress in a laminate to implement a failure constraint. Deformation and stress variations in the panel will depend on the in-plane boundary conditions applied on the longitudinal and transverse edges, $y = \pm b/2$ and x= $\pm a/2$. Here, a straight-edge boundary that can expand or contract in the transverse and longitudinal directions is enforced.

For the type-1 laminate; the fiber orientation angle θ is a function of the x-coordinate only $[0\pm<T_0|T_1>]_{2S}$, and is subjected to a non-uniform temperature profile. In Figure 11, the maximum axial stress resultant of the panels is normalized by the maximum axial stress resultant for a straight-fiber $\theta=0^\circ$ laminate, and are shown as a function of the right edge displacement in the longitudinal direction normalized by the edge width. The heavy green line in the figure is the locus of results for constant-stiffness straight-fiber format panels, and shows the variation of both the maximum stress resultant and plate right edge displacement

as the fiber orientation angle is changed from $0°$ to $90°$. The lowest normalized stress resultant for this square panel with straight fibers and forced straight edges is 0.468 and corresponds to a $±45°$ laminate with normalized longitudinal deflection value of about 0.084. For variable-stiffness panels a family of curves corresponding to various values of T_1 (from $0°$ to $90°$ with increments of $15°$) is shown in Figure 11. Each curve is generated by varying the value of T_0 between $0°$ and $90°$ for a given value of T_1 as labeled in the figure. Intersection of these curves with the curve for the straight-fiber panel is a constant-fiber angle panel where T_1 is equal to T_0. The lowest normalized value of the stress resultant is 0.126, and is obtained for a variable stiffness configuration of $T_0 = 0°$ and $T_1 = 45°$. The corresponding normalized longitudinal deflection of this panel is about 0.084, which is 73% lower than the lowest value of 0.468 obtained with a straight-fiber $±45°$ configuration. Most variable stiffness panels with $T_0 = 0°$ have a higher stress resultant than straight-fiber configurations for T_1 in the range of $0°$ to $45°$.
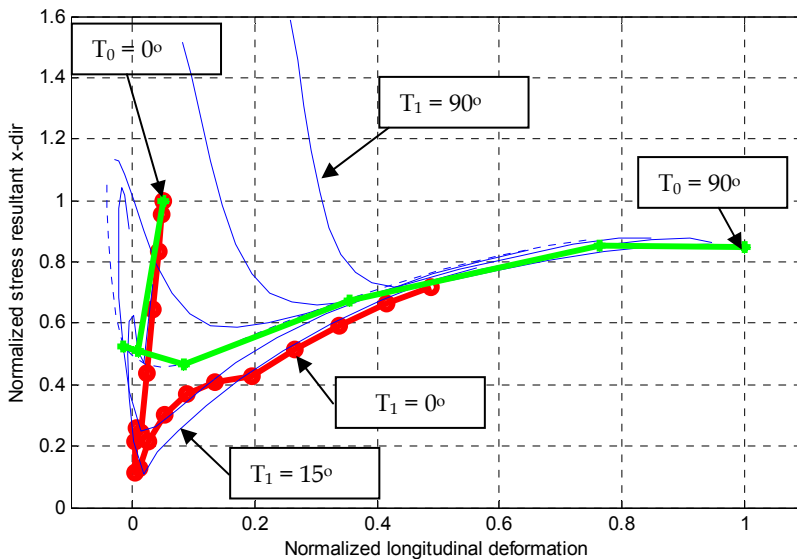

Fig. 11. Normalized longitudinal stress resultant for $[0±<T_0|T_1>]_{2S}$

For the type-2 laminate; the fiber orientation θ is a function of both the x- and y-coordinates, where $\theta=[0 ±<T_0/T_1>/90± <T_0/T_1>]_S$. A non-uniform temperature profile is again applied to the panels. The maximum axial stress resultant of panels normalized by maximum axial stress resultant for straight-fiber laminate $\theta=0°$ are shown in Figure 12 as a function of the right edge displacement in the longitudinal direction normalized by the edge width. The heavy green line in the figure is for constant-stiffness, straight-fiber format panels, and shows the variation of both the maximum stress resultant and plate right edge displacement as the fiber orientation angle ranges from $0°$ to $90°$. The lowest normalized stress resultant for this square panel with straight fibers and forced straight edges is 0.573, and corresponds to a $±45°$ laminate. The normalized longitudinal deflection value is constant at a value of 1 for all straight-fiber configurations.

For variable-stiffness panels a family of curves corresponding to various values of T_1 (from 0° to 90° in increments of 15°) is plotted in Figure 12. The lowest normalized value of stress-resultant is 0.185, and is obtained for a variable stiffness configuration of $T_0 = 85^o$ and $T_1 = 0^o$, with normalized longitudinal deflection value of about 1.127. This value is 68% lower than the lowest value of 0.577 obtained with a straight-fiber configuration, but with 12% increase of normalized longitudinal deformation. Most variable stiffness panels with $T_0 = 0^o$ and T_1 in the range of 0° to 45° have a higher stress resultant than the corresponding straight-fiber configurations.
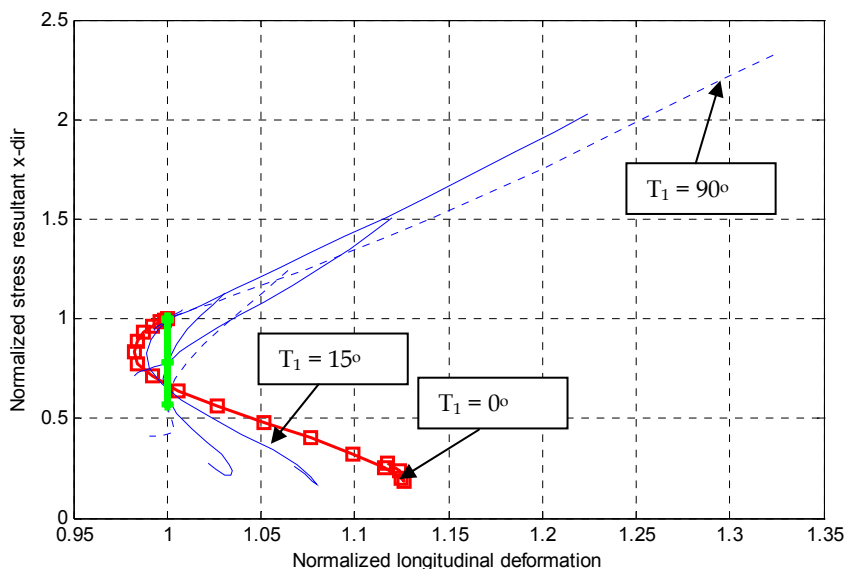
Fig. 12. Normalized longitudinal stress resultant for $[0 \pm <T_0/T_1>/90\pm <T_0/T_1>]_S$

6. Thermal testing of variable stiffness laminates

The thermal-structural responses of two variable stiffness panels and a third cross-ply panel are evaluated under thermal loads. A brief description of the variable stiffness panels and their fiber orientation angles is given, along with an overview of the thermal test setup and instrumentation. Results of these tests are presented and discussed, and include measured thermal strains and calculated coefficients of thermal expansion.

6.1 Fiber tow path definition

The layups of the three composite panels tested in this study are described herein. The two variable stiffness panel layups are $[\pm45/(\pm\theta)_4]_s$, where the steered fiber orientation angle θ varies linearly from $\pm60^o$ on the panel axial centerline, to $\pm30^o$ near the panel vertical edges 30.5 cm away. The curvilinear tow paths that the fiber placement machine followed during fabrication of these variable stiffness panels are shown in Figure 13. One panel has all 24, 0.32-cm-wide tows placed during fabrication. This results in significant tow overlaps and thickness buildups on one side of the panel, and therefore it is designated as the panel with

overlaps. The fiber placement system's capability to drop and add individual tows during fabrication is used to minimize the tow overlaps of the second variable stiffness panel, which is designated as the panel without overlaps. The third panel has a straight-fiber [±45]$_{5s}$ layup and provides a baseline for comparison with the two variable stiffness panels. The overall panel dimensions are 66.0 cm in the axial direction, and 62.2 cm in the transverse dimension, as indicated by the dashed lines in the figure. Further details of the panel construction are given in (Wu, 2006).

6.2 Test setup and instrumentation

The thermal test was performed in an insulated oven with feedback temperature control. Electrical resistance heaters and a forced-air heater unit were used to heat the enclosure. Perforated metal baffles were used to evenly distribute hot air over the back surface of the panel. The oven's front was glass to allow observation of the panel using shadow moiré interferometry. The panel was supported inside the oven with fixtures that restricted its rigid-body motion but allowed free thermal expansion. The panel was placed on two small quartz rods that prevented direct contact with the lower heated platen. The panel surfaces were supported between quartz cones and spring-loaded steel probes with low axial stiffnesses.
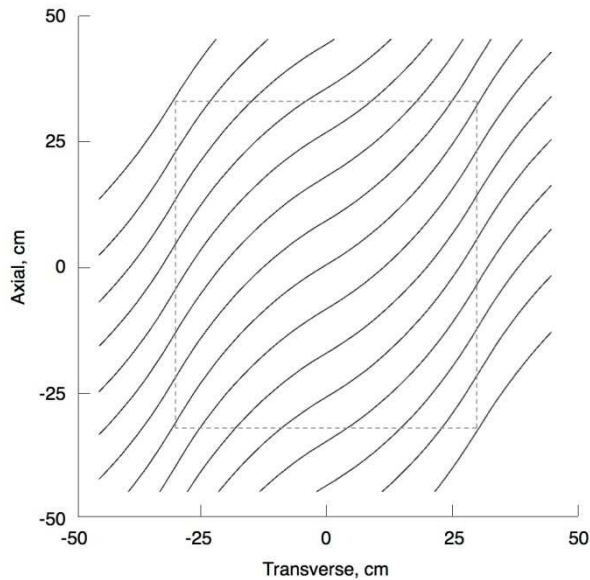

Fig. 13. Variable stiffness panel tow paths.

Each composite panel was gradually heated from room temperature up to approximately 65 °C. A feedback control system provided closed-loop, real-time thermal control based on readings from five K-type thermocouples on the heated platens and air inlet surrounding the panel. These separate data were then averaged into a single temperature provided to the control system. The thermocouples used in this study have a measurement uncertainty of ±1 °C. For a thermal test, the control temperature inside the oven was first raised to 32 °C and

held there for 5 minutes. After the hold period, the control temperature was raised at 1 ºC/min. to a maximum of 65 ºC and held there for 20 minutes before the test was ended. The solid line in Figure 14 shows the average of the five control thermocouples plotted against time for a typical test.
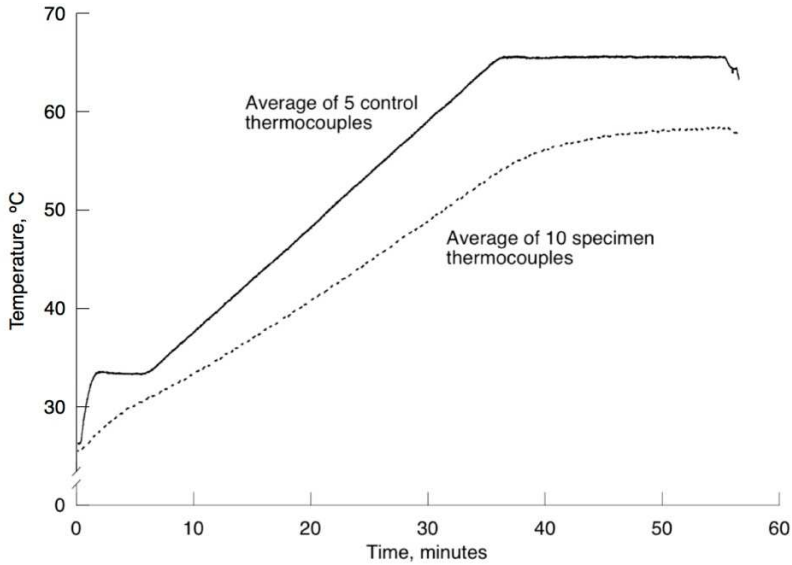
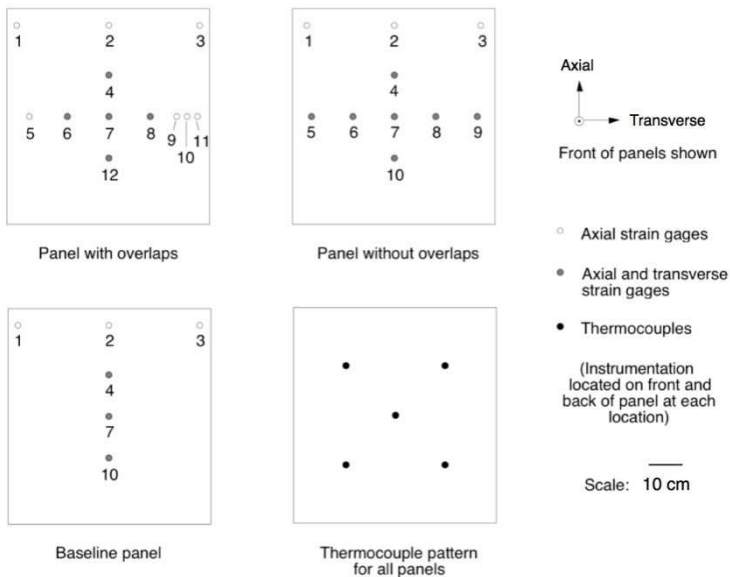Fig. 14. Temperature profiles for thermal tests.

Fig. 15. Composite panel instrumentation.

The panel response was measured during the thermal test with thermocouples and strain gages, and these data were collected using a personal computer-based system. Panel front and back surface temperatures were measured with five pairs of K-type thermocouples. The average panel temperature is shown as a function of time as the dashed line in Figure 14. The thermocouples, denoted as black-filled circles, are located at the corners and center of a 30.5-cm square centered on the panel, as shown in Figure 15.

Back-to-back pairs of electrical-resistance strain gages (each with a nominal ±1 percent measurement error) are bonded to the panel surfaces using the procedures described in (Moore, 1997). The locations of the strain gage pairs on each panel are also shown in Figure 15. The strain gages measure either axial strains (the open circles in the figure), or both axial and transverse strains (the gray filled circles), and are deployed along the top edge, and axial and transverse centerlines of the panels. The closely spaced axial gage pairs (locations 9, 10 and 11) on the panel with overlaps span a region of varying laminate thickness along the transverse centerline. In addition to the axial gage pairs along the upper edge of the baseline panel, biaxial gages are fitted at locations 4, 7 and 10 along the axial centerline.

6.3 Test results

The heating profile shown in Figure 14 is applied to the panels, and the resulting panel thermal response is measured. An initial thermal cycle is performed for each panel to fully cure the adhesives used to attach the strain gages to the panels. Since the strain gage response is dependent on both its operating temperature and the motion of the surface to which it is bonded, the thermal output of the strain gages themselves (Anon., 1993; Kowalkowski et al., 1998) must first be determined. Strain data are recorded for gages bonded to Corning ultralow-expansion titanium silicate (coefficient of thermal expansion $0 \pm 3.06 \times 10^{-8}$ cm/cm/$^{\circ}$C) blocks that are subjected to the same thermal loading. After completion of each thermal test, this thermal output measurement is then subtracted from the total (apparent) strain of each strain gage recorded during the test to obtain the actual mechanical strains presented below.

6.3.1 Variable stiffness panels

Measured axial and transverse strains at the center (gage location 7) of the panel with overlaps are plotted against the panel temperature in Figure 16 for a representative thermal test. The plotted strains on the front and back panel surfaces are proportional to the temperature, and are qualitatively similar to the responses at the other panel gage locations. The membrane strain at the laminate mid-plane is defined as the average strain from a back-to-back gage pair. The panel's local coefficient of thermal expansion (CTE) at that gage location is then defined as the linear best-fit slope of the membrane strain as a function of temperature. Using the panel center strains shown in Figure 16, the measured axial CTE there is 9.11×10^{-6} cm/cm/$^{\circ}$C, and the transverse CTE is 0.11×10^{-6} cm/cm/$^{\circ}$C (units of 1×10^{-6} cm/cm are denoted as µε or microstrain). Note that these local CTEs for the variable stiffness panels are dependent on the non-uniform fiber orientation angles, and may not be equal to straight-fiber CTEs calculated using classical lamination theory.

The maximum measured strains at each of the 12 gage locations on the panel with overlaps are plotted in Figure 17, with the corresponding axial CTEs shown in Figure 18. The axial CTEs increase from –3.98 µε/$^{\circ}$C near the edges ($\theta=\pm30^{\circ}$) to 10.67 µε/$^{\circ}$C along the axial centerline ($\theta=\pm60^{\circ}$). Transverse CTEs are also plotted in the figure and range from –0.94 to 1.35 µε/$^{\circ}$C. In

general, the fiber-dominated ±30º layups near the panel edges have low axial CTEs and high transverse CTEs. The opposite is true for the matrix-dominated ±60º laminates on the panel axial centerline, which have high axial CTEs and low transverse CTEs.
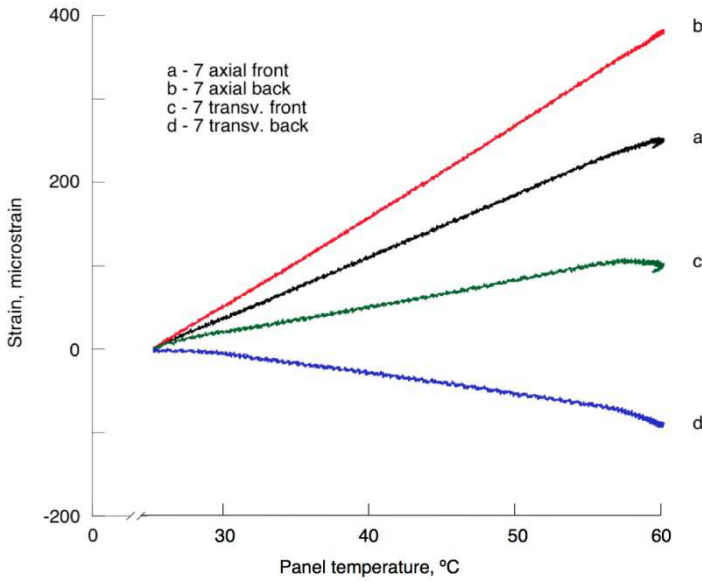

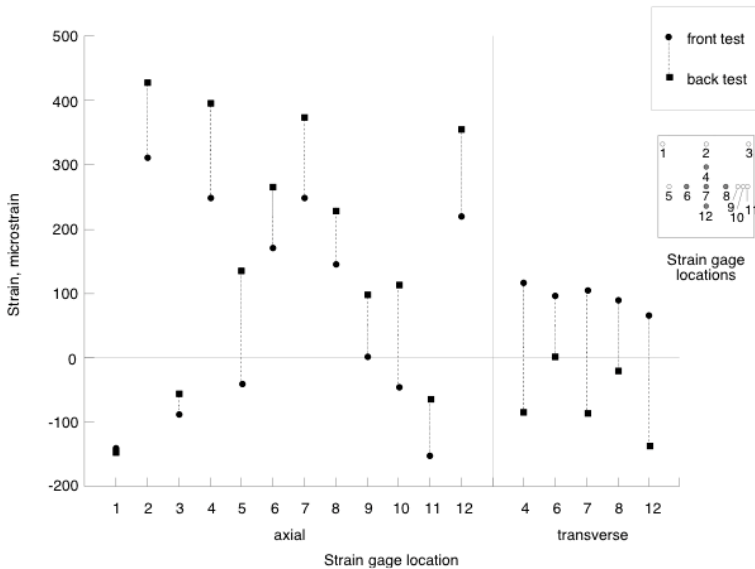Fig. 16. Strain vs. temperature at center of panel with overlaps.

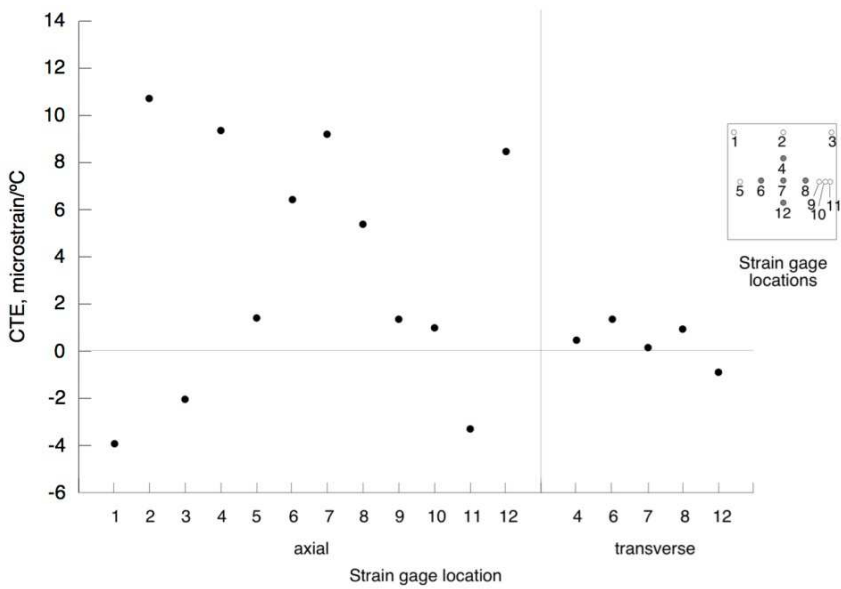
Fig. 17. Maximum strains for panel with overlaps.

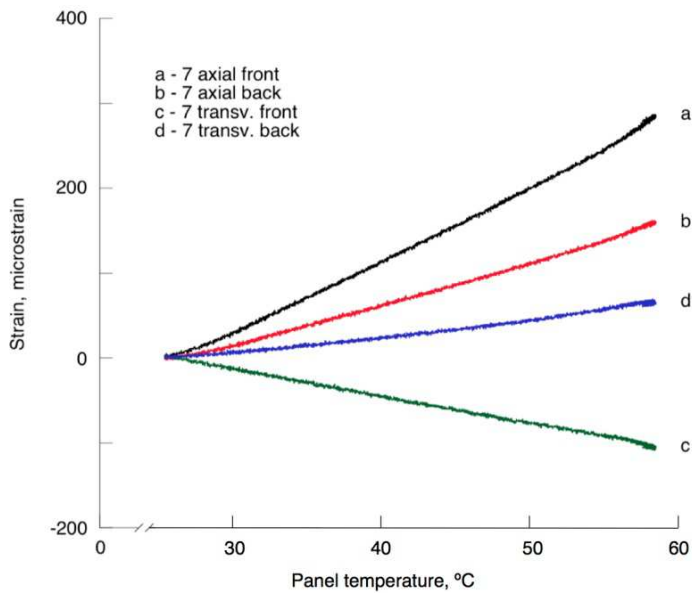Fig. 18. CTEs for panel with overlaps.

Fig. 19. Strain vs. temperature at center of panel without overlaps.

The 20-ply laminate on the transverse centerline 12.7 cm on either side of the panel center has a [±45/(±48)4]s layup. However, the measured axial CTEs (6.35 and 5.33 µε/°C) at gage locations 6 and 8 there are much higher than the corresponding transverse CTEs (1.35 and 0.92 µε/°C). Since the CTEs of an [±45]5s orthotropic cross-ply laminate should all be equal, the observed differences strongly suggest that the variable stiffness laminate CTEs can be highly sensitive to relatively small changes in the fiber orientation angles.
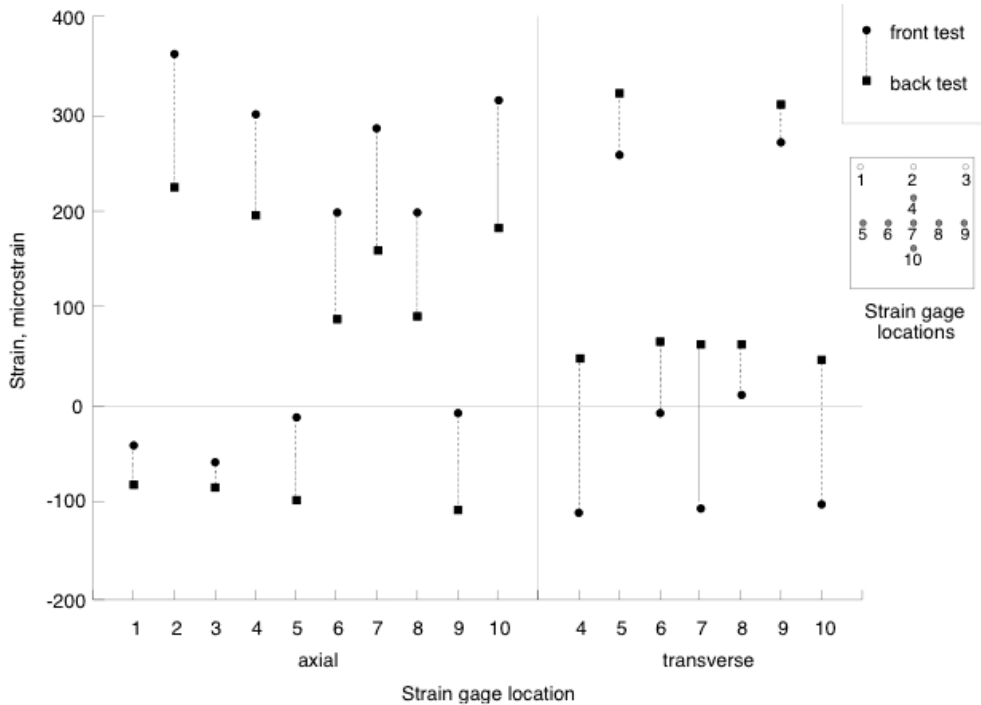
Fig. 20. Maximum strains for panel without overlaps.

Measured axial and transverse strains on the front and back surfaces of the center of the panel without overlaps are shown plotted against the corresponding panel temperature in Figure 19. The axial and transverse strains at the maximum test temperature at each of the 10 strain gage locations on this panel are shown in Figure 20. The axial and transverse CTEs plotted in Figure 21 are then calculated from the membrane strains. Axial CTEs for the panel without overlaps range from –2.14 µε/°C near the panel edges to 9.16 µε/°C along the axial centerline, with transverse CTEs ranging from –0.79 µε/°C on the axial centerline to 9.07 µε/°C on the transverse centerline near the panel edge. The CTEs for the panel without overlaps are much more symmetric with respect to the panel axial and transverse centerlines

than those described previously for the panel with overlaps. However, similar qualitative trends are observed in the plotted CTEs for both panels.
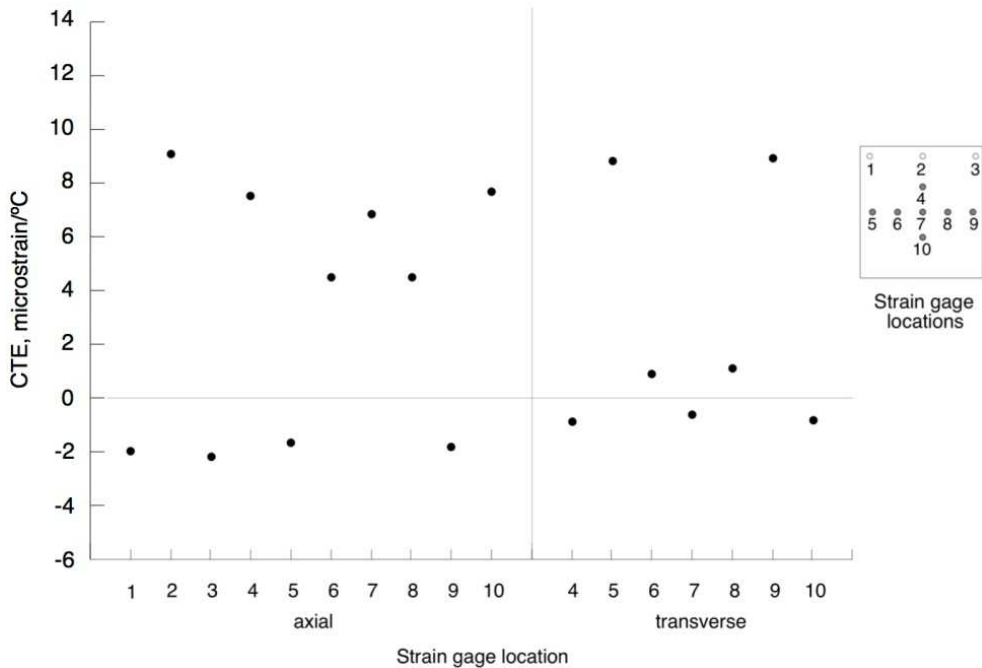

Fig. 21. CTEs for panel without overlaps.

6.3.2 Baseline panel

Front and back surface axial and transverse strains at the baseline panel center are plotted as functions of the panel temperature in Figure 22. The measured strains are linear and very nearly equal, which is to be expected since the [±45]5s layup has the same response in both the axial and transverse directions. The range of measured CTEs for the baseline panel is from 2.34 to 3.40 µε/°C, with an average CTE of 2.92 µε/°C. The corresponding standard deviation is 0.32 µε/°C, resulting in an 11 percent coefficient of variation. The maximum temperature for the baseline panel thermal test is about 3.9 °C lower than the maximum temperature for the variable stiffness panels because the heating profile was terminated when the temperature reached 65 °C.
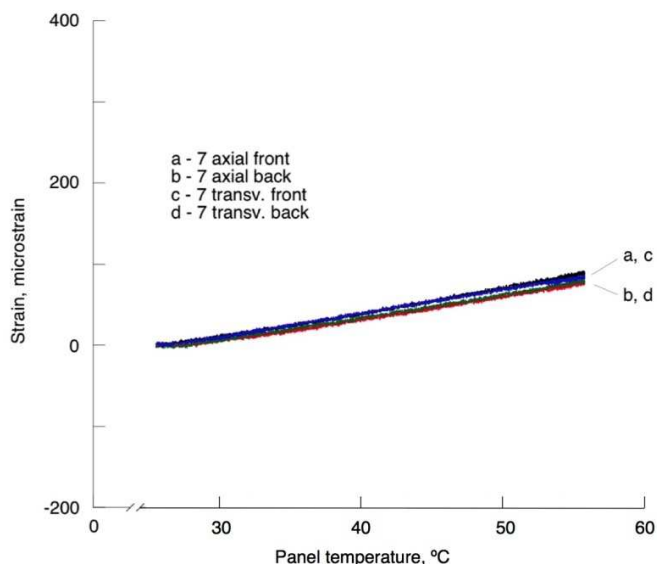
Fig. 22. Strain vs. temperature at center of baseline panel.

6.4 Summary

The measured strain response at each gage location on each of the composite panels is generally linear with increasing temperature. The membrane strain at each gage location is defined and used to compute the laminate CTE at that location. The measured axial CTEs for both variable stiffness panels are lowest near the panel edges and increase to their maximum values along the axial centerline, while the transverse CTEs show the opposite behavior. This corresponds to the fiber-dominated ±30° layup towards the panel edges and a matrix-dominated ±60° layup on the axial centerline. For a given orientation, the measured CTEs along the panel axial centerlines are all fairly close to one another. This is as expected, since the fiber orientation angle varies along the panel transverse axis, with only the ply shifts contributing to any axial fiber orientation angle variation.

7. References

Abdalla, M, Gürdal, Z and Abdelal, G. (2009). Thermomechanical response of variable stiffness composite panels. *Journal of Thermal Stresses*, Vol. 32, No. 1, pp. (187 – 208).

Anon. (1993). Strain Gage Thermal Output and Gage Factor Variation with Temperature. *TN-504-1, Measurements Group*, Inc., Raleigh, North Carolina.

Banichuk, NV. (1981). Optimization Problems for Elastic Anisotropic Bodies. *Archive of Mechanics*, 33, 1981, pp. (347-363).

Banichuk, NV and Sarin, V. (1995). Optimal Orientation of Orthotropic Materials for Plates Designed Against Buckling. *Structural and Multidisciplinary Optimization*, Vol. 10, No. 3-4, 1995, pp. (191-196).

Bogetti, T. (1989). Process-Induced Stress and Deformation in Thick-Section Thermosetting Composites. *Technical Report CCM-89-32*, Center for Composite Materials, University of Delaware, Newark, Delaware, 1989.

Bogetti, T and Gillespie, J. (1992). Process-Induced Stress and Deformation in Thick-Section Thermoset composite Laminates", *Journal of Composite Materials, Vol.* 26, No. 5, pp. (626-660).

Cole, K, Hechler, J and Noël, D. (1991). A New Approach to Modelling the Cure Kinetics of Epoxy Amine Thermosetting Resin. 2. Application to a Typical System Based on Bis[4-diglycidylamino)phenyl]methane and Bis(4-aminophenyl) Sulphone", *Macromolecules.* Vol. 24, No. 11, pp. (3098-3110).

Dusi, M, Lee, W, Ciriscioli, P and Springer, G. (1987). Cure Kinetics and Viscosity of Fiberite 976 Resin," *Journal of Composite Materials.* Vol. 21, No. 3, pp. (243-261).

Duvaut, G, Terrel, G, Léné, F and Verijenko, V. (2000). Optimization of Fiber Reinforced Composites. *Composite Structures*, Vol. 48, 2000, pp. (83-89).

Gürdal, Z and Olmedo, R. (1993). In-Plane Response of Laminates with Spatially Varying Fiber Orientations: Variable Stiffness Concept. *AIAA Journal*, Vol. 31, (4), pp. (751-758), 0001-1452.

Gürdal, Z, Haftka, RT and Hajela, P. (1999). *Design and Optimization of Laminated Composite Materials*. John Wiley & Sons, Inc., New York, NY.

Gürdal, Z, Tatting, BF and Wu, KC. (2008). Variable stiffness composite panels: Effects of stiffness variation on the in-plane and buckling response. *Composite: Part A*, Vol. 39, 2008, pp. (911-922).

Hetnarski, RB. (1996). *Thermal stresses (I–IV)*. Amsterdam: Elsevier Science Pub. Co.

Hughes, T, Levit, I and Winget, J. (1982). Unconditionally stable element-by-element implicit algorithm for heat conduction analysis. U.S. Applied Mechanics Conference, Cornell University, Ithaca, USA.

Johnston, A. (1997). *An Integrated Model of the Development of Process-Induced Deformation in Autoclave Processing of Composite Structures*. PhD dissertation, University of British Columbia.

Levitsky, M and Shaffer, B. (1975). Residual Thermal Stresses in a Solid Sphere Cast From a Thermosetting Material. *Journal of Applied Mechanics*, pp. (651-655).

Kowalkowski, M, Rivers, HK and Smith, RW. (1998). Thermal Output of WK-Type Strain Gauges on Various Materials at Elevated and Cryogenic Temperatures. *NASA TM-1998-208739*, October 1998.

Lee, W, Loos, A and Springer, S. (1982). Heat of Reaction, Degree of Cure, and Viscosity of Hercules 3501-6 Resin", *Journal of Composite Materials.* Vol. 16, pp. (510-520).

Mittler, G, Klima, R, Alapin, B, et al. (2003). Determination and application of thermo-mechanical characteristics for the optimization of refractory linings. *STAHL UND EISEN* Vol. 123, No. 11 pp. (109–12).

Moore, T. (1997). Recommended Strain Gage Application Procedures for Various Langley Research Center Balances and Test Articles. *NASA TM-110327*, March 1997.

Obata, Y and Noda, N. (1993). Unsteady thermal stresses in a functionally gradient material plate - Analysis of one-dimensional unsteady heat transfer problem. Japan Society of Mechanical Engineers, Transactions A (ISSN 0387-5008), Vol. 59, No. 560, pp. (1090-1096).

Olmedo, R and Gürdal, Z. (1993). Buckling Response of Laminates with Spatially Varying Fiber Orientations, Proceedings of the 34th AIAA/ASME/ASCE/AHS/ASC Structures, Structural Dynamics and Materials (SDM) Conference, La Jolla, CA, April 1993.

Pedersen, P. (1991). On Thickness and Orientation Design with Orthotropic Materials. *Structural Optimization*, Vol. 3, 1991, pp. (69-78).

Pedersen, P. (1993). Optimal Orientation of Anisotropic Materials, Optimal Distribution of Anisotropic Materials, Optimal Shape Design with Anisotropic Materials, Optimal Design for a Class of Non-linear Elasticity. *Optimization of Large Structural Systems*, Ed. Rozvany, G. I. N., Vol. 2, 1993, pp. (649-681).

Scott, P. (1991). Determination of Kinetic Parameters Associated with the Curing of Thermoset Resins Using Dielectric and DSC Data", *Composites: Design, Manufacture, and Application, ICCM/VIII*, Honolulu, 1991.

Segerlind, LJ. (1984). *Applied Finite Element Analysis*. John Wiley & Sons.

Setoodeh, S, Abdalla, M and Gürdal, Z. (2006). Design of variable–stiffness laminates using lamination parameters. *Composites Part B: Engineering*. Vol. 37, No. 4-5, pp. (301-309).

Setoodeh, S, Abdalla, M and Gürdal, Z. (2007). Design of variable stiffness composite panels for maximum fundamental frequency using lamination parameters. *Composite Structures*. Vol. 81, No. 2, pp. (283-291).

Setoodeh, S, Abdalla, M, IJsselmuiden, S and Gürdal, Z. (2009). Design of variable-stiffness composite panels for maximum buckling load. *Composite Structures*. Vol. 87, No. , pp. (109-117).

Thornton, EA. (1992). *Thermal structures and materials for high-speed flight*. American Institute of Aeronautics and Astronautics.

Trujillo, D. (1977). An unconditionally stable explicit algorithm for structural dynamics. *International Journal of Numerical Methods Engineering*, Vol. 1, pp. (1579-1592).

Twardowski, T, Lin, S and Geil, P. (1993). Curing in Thick Composite Laminates: Experiments and Simulation", *Journal of Composite Materials.* Vol. 27, No. 3, pp. (216-250).

White, S and Hahn, H. (1992). Process Modelling of Composite Materials: Residual Stress Development during Cure. Part I. Model Formulation", *J. of Composite Materials.* Vol. 26, No. 16,pp. (2402-2422).

Wu, KC. (2006). Thermal and Structural Performance of Tow-Placed, Variable Stiffness Panels. ISBN 1-58603-681-5, *Delft University Press/IOS Press*, Amsterdam, The Netherlands, 2006.

Zienkiewicz, O, Hinton, E, Leung, K and Taylor, R. (1980). Staggered time marching schemes in dynamic soil analysis and a selective explicit extrapolation algorithm. Second International Symposium on Innovative Numerical Analysis in Applied Engineering Sciences, Canada.

Heat Transfer - Engineering Applications

Edited by Prof. Vyacheslav Vikhrenko

Heat transfer is involved in numerous industrial technologies. This interdisciplinary book comprises 16 chapters dealing with combined action of heat transfer and concomitant processes. Five chapters of its first section discuss heat effects due to laser, ion and plasma-solid interaction. In eight chapters of the second section engineering applications of heat conduction equations to the curing reaction kinetics in manufacturing process, their combination with mass transport or ohmic and dielectric losses, heat conduction in metallic porous media and power cables are considered. Analysis of the safety of mine hoist under influence of heat produced by mechanical friction, heat transfer in boilers and internal combustion engine chambers, management for ultrahigh strength steel manufacturing are described in this section as well. Three chapters of the last third section are devoted to air cooling of electronic devices.

How to reference

In order to correctly reference this scholarly work, feel free to copy and paste the following: